3-DoF Wearable, Pneumatic Haptic Device to Deliver Normal, Shear, Vibration, and Torsion Feedback

Kyle T. Yoshida, Cara M. Nunez, *Student Member, IEEE*, Sophia R. Williams, *Student Member, IEEE*, Allison M. Okamura, *Fellow, IEEE*, and Ming Luo, *Member, IEEE*

***Abstract*— Haptic devices worn on the forearm have the ability to provide communication while freeing the user's hands for manipulation tasks. We introduce a multi-modal haptic device with a rigid rotational housing and three soft fiber-constrained linear pneumatic actuators. Soft pneumatic actuators are used because of their compliance, light weight, and simplicity, while rigid components provide robust and precise control. The soft pneumatic actuators provide linear horizontal and vertical movements, and the rigid housing, affixed to a motor, provides rotational movement of the tactor. The device can produce normal, shear, vibration, and torsion skin deformation cues by combining the movement of the soft pneumatic actuators with the rotational housing. The tactor is able to provide a shear force of up to 0.47 N and a normal force of up to 1.3 N. To elucidate the physical design principle and the actuation strategy, the static force and displacement of the soft tactor are modeled as a function of material, design parameters, and pressure. The models were validated experimentally.**

I. Motivation

Wearable haptic devices offer the ability to convey tactile information to a human user in a compact form-factor that allows the user to move freely in their environment and leaves their hands free to perform other tasks. Providing haptic feedback in this manner could be useful for applications in virtual environments or to enhance human-human, human-robot, and human-virtual agent communication. To date, wearable haptic feedback has been proven effective for encoding speech [1], providing directional cues [2], [3], translating audio to tactile cues [4], translating video to tactile cues [5], and in creating pleasant stroking sensations for relaying social haptic cues [6].

Hairy skin, such as the skin on the forearm, contains various mechanoreceptors that respond to different stimuli. For example, Pacinian corpuscles respond to rapid vibration, Merkel cells are sensitive to pressure, Meissner corpuscles respond to dynamic skin deformation such as skin-slip, Ruffini endings are sensitive to skin stretch, and C-tactile afferents respond to stroking [7], [8]. Traditionally, wearable haptic devices are uni-modal, or designed to create sensations with only one mode of actuation. However, multi-modal haptic devices, such as Rice University's MISSIVE [9], target multiple mechanoreceptors and create sensations with several different actuation techniques across multiple contact areas. In contrast, our device offers multi-modal haptic cues in a single contact area.

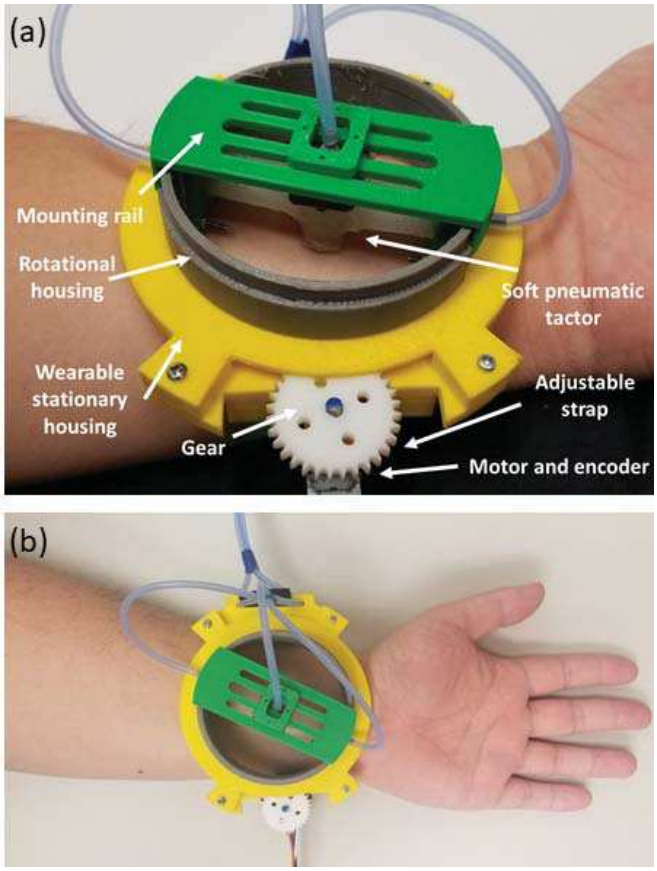

Fig. 1. The wearable haptic device is comprised of three fiber-constrained soft linear pneumatic actuators for normal and lateral displacement and one DC gear motor for rotation. The combination of soft actuator and DC motor motions can create normal, shear, vibration, and torsion cues. A close-up view of the device is shown in (a), and the device on worn on the forearm is shown in (b).

Soft wearable devices offer many advantages compared to traditional rigid haptic devices. However, the design of soft wearable devices is challenging, particularly for stimulation in certain directions. For example, creating rotational motion is simpler with traditional rigid actuators, like motors, than with soft actuators. In contrast, it is easy to create linear motion with soft actuators, but difficult for rigid actuators because it requires additional components such as a linear rail, ball bearing, and a lead screw, which can affect the

This work was supported in part by National Science Foundation grant 1830163 and the National Science Foundation Graduate Fellowship Program.

K. T. Yoshida, C. M. Nunez, A. M. Okamura, and M. Luo are with the Mechanical Engineering Department, Stanford University, CA 94305, USA. (e-mail: kyle3@stanford.edu, nunezc@stanford.edu okamura@stanford.edu, mingluo@stanford.edu)

C. M. Nunez is with the Bioengineering Department, Stanford University, CA 94305, USA. (e-mail: nunezc@stanford.edu)

S. R. Williams is with the Electrical Engineering Department, Stanford University, CA 94305, USA. (e-mail: sophiarw@stanford.edu)

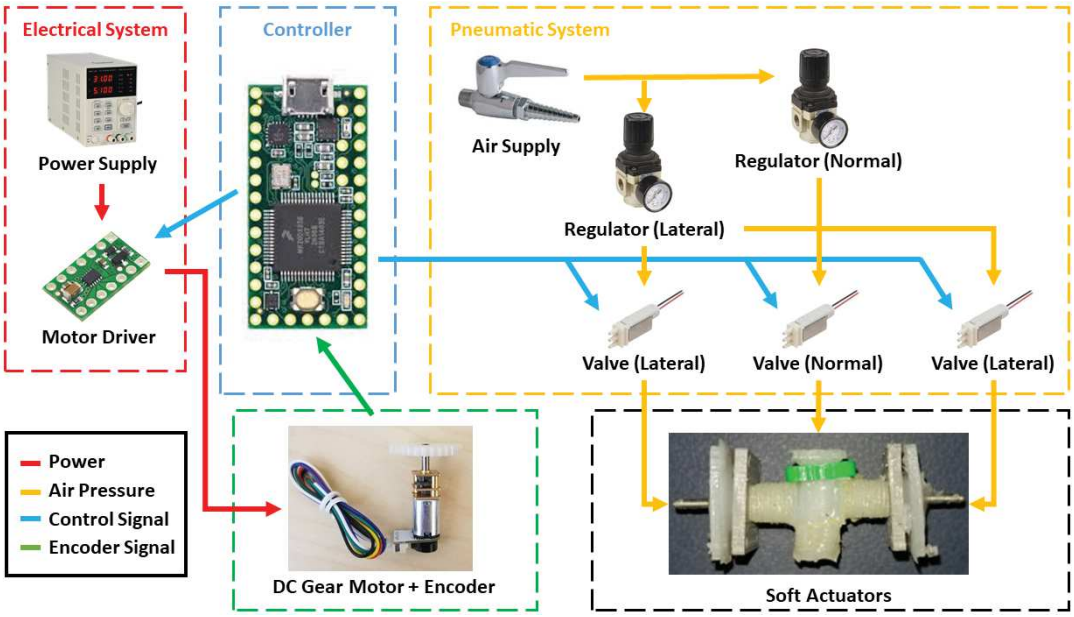

Fig. 2. The wearable haptic device is composed a pneumatic system that delivers pressure to the lateral and normal actuators and an electrical system that controls DC motor movements. Combining the DC motor movements with the lateral and normal motions of the actuators creates a 3-DoF haptic device.

system speed and cost. The combination of soft and rigid components to make a soft-rigid hybrid device provides flexibility and adaptability in creating a light weight and user friendly interface through the use of soft materials, while also allowing for robust, controlled movement through rigid components and movement of motors.

In this paper, we present a new 3-degree-of-freedom (3-DoF) wearable, pneumatic haptic device that can provide normal, shear, vibration, and torsion feedback to the forearm (Fig. 1). The device uses a combination of pneumatic and motor control inputs in sequence to create these haptic cues. The normal forces, shear forces, and lateral displacement of the soft actuators were analytically modeled and verified to assist in making future design decisions.

II. Prior Work

Researchers have begun investigating how to best design and build soft wearable haptic devices. Many of these designs incorporate pneumatic actuation. For example, the WRAP [10] and the HapWRAP [11] actuate plastic pouches to provide accurate directional cues. The SPA skin [12] is a distributed array that uses pneumatic actuation to relay different patterns via vibration. All of these devices use multiple contact points, with a single DoF. The goal of our previous work, the 2-DoF soft haptic device [3], was to develop a device that could achieve multiple DoF with a single contact point to relay directional cues. Our 3-DoF multi-modal haptic device improves upon this previous design. From our previous work, we experienced first-hand many of the challenges associated with using soft materials to create wearable haptic devices. Specifically, using soft materials in the design of a wearable device does not offer as strong grounding as rigid materials, which affects the reaction forces and sensations provided by the device. In order to address this issue, we emphasized creating a soft-rigid hybrid device that could effectively use rigid components for mounting and grounding, and soft components for comfort and actuation. Similar to our previous device, we designed our 3-DoF device to be able to provide shear forces between 0.2-1 N with displacements of 1-5 mm based on prior work by Paré et al. [13] and internal pilot studies. While our previous device design was limited to relaying directional cues via skin stretch in only the cardinal and intermediate directions, our new design allows for specifically controlled directions by incorporating a motor and transmission system to rotate the device to multiple angles. We also introduced an additional degree of freedom such that the tactor makes and breaks contact with the skin through pressurization and depressurization of the center actuator.

Comparatively, the MISSIVE system provides simultaneous multi-modal feedback to the upper arm with high information transfer rates, but does so with multiple contact points [9]. The MISSIVE system consists of a distal band that houses four vibrotactors to relay vibration cues and a proximal band that is designed like the Rice Squeeze Band [14] to squeeze the user's arm. Attached to the proximal band is also a Rice Haptic Rocker [15] to provide skin stretch cues. In contrast, our design provides different forms of haptic feedback to the same location, reducing the overall contact surface area with the skin. Our design allows for device simplification and improved wearability due to its single contact region, while its multi-modal haptic cues can relay more information to the user.

III. Design and Fabrication

The haptic device uses a hybrid actuation system composed of the soft pneumatic actuator system and the electrical DC motor driven system as shown in Fig. 2. The T-shaped soft tactor, as seen in Fig. 3, is made from three fiber-constrained soft linear pneumatic actuators using silicone

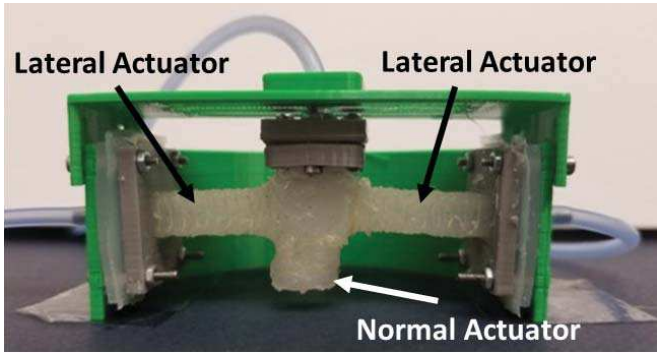

Fig. 3. The tactor consists of three fiber-constrained soft linear actuators mounted to the rigid housing. Contact is created by pressurizing the normal actuator.

rubber (Ecoflex 00-30, Smooth-On) [16]. The soft actuator is created by casting the rubber into a cylindrical mold then wrapping thread around its exterior (threading) to constrain outward motion. This tactor contains two lateral actuators and one normal actuator. Motion for one-dimensional shear displacement comes from actuating the pre-stretched lateral actuators, and motion for normal indentation comes from actuating the normal actuator. The pressure regulators for normal and shear motion are decoupled, to control normal and shear independently. In contrast to our previous 2-DoF haptic device [3], the tactor breaks contact with the skin by lifting the normal actuator via depressurization. This avoids unwanted skin cues when the device re-orients itself. The actuator can move between pressurized and unpressurized states in 0.4 seconds.

In addition to the linear motion from the normal and lateral actuators, the inner rotational housing provides angular movement. The rotational housing has a laser cut spur gear attached to its outer circumference, which interacts with a smaller spur gear attached to the motor. Rotational movement is created by a micrometal gearmotor (Pololu, 50:1, MP 6V) with an attached encoder (Pololu, 12 CPR, 2.7-18 V). The full rotational system has a resolution of 0.26°, a 112.5:1 gear ratio, an angular velocity of 1.5 rotations per second, and a stall torque of 1.215 kg-cm. Using feedback control, the motor rotates the housing to a desired angular position to create vibrations or torsion action on the skin.

The wearable housing constrains the inner rotational housing while also providing the mounting areas for the motor and a strap. The housing has two slot holes, allowing a nylon strap with velcro to be passed through for firm attachment to the arm. The mounting rail attaches to the end cap of the normal actuator and sides of the rotational housing to constrain vertical motion, while still allowing the tactor center to slide laterally when pressurized. The mounting rail height can be adjusted with respect to the rotational housing to control the initial tactor head distance to the skin to ensure that the tactor head loses contact, when depressurized, to prevent the user from noticing extraneous cues. Assembled with actuators, housing, motors, and the strap, the total device mass is 82 g with an outer diameter of 11.3 cm and height of 3 cm.

IV. Static Modeling

We developed then verified a model for the soft actuator that we can use for designing future devices. The model uses the actuator material, length, cross sectional area, and input pressures to estimate the device's lateral displacement and ability to generate normal force.

A. Model

The static model for the tactor is composed of three static actuator models. The normal force model was straightforward, since there is no significant change in length of the normal actuator and a fixed cross sectional area during pressurization. The actuator's lateral displacement model was determined using force balance equations between two static soft linear actuator models that balance pressure and silicone material forces.

A similar static analytical model of a soft linear actuator is given in [16]. This model estimates the extension of the soft linear actuator under a given internal pressure and load. However, the previous model is complex and can lead to numerical errors; we found that it can be simplified because some variables have minimal effect on the output of our device. Therefore, the following assumptions were made for the models in this study:

1) The outer diameter of the soft linear actuator is constant for all pressures: We assume that the outer diameter of the soft linear actuator in its unstretched and pressurized states are the same by assuming that the threading effectively constrains the actuator for the short actuation distances used in this device.

2) The soft material model is constant with respect to cross-sectional area: The Young's modulus of the soft material in the model was used instead of the third-order Ogden model in [16] because of the relatively short actuation distance. For larger displacements, a higher-order model would be needed.

3) The connection between the two lateral actuators is rigid: The middle connection piece, above the normal actuator and between the lateral actuators, was treated as a rigid component, because it was made using a stiffer material (Dragonskin 10, Smooth-On). This piece has a hole to channel air to the normal actuator, but has minimal expansion when pressurized.

4) The sum of the two lateral actuator lengths is constant and only linear motion occurs: Because the lateral actuators are attached between rigid components, we assume that the sum of their lengths is constant. This assumption also implies that there is no significant bending or twisting, which was confirmed visually; the guide rail constrains unwanted motion.

Table I and Fig. 4 summarize the parameters used in the tactor model. When the normal actuator is pressurized and in contact with a surface, its length cannot increase, so material forces opposing its motion are negligible. Therefore, the model for normal indentation force F_n is:

$$F_n = PH_{in}W_{in}, \tag{1}$$

TABLE I

PARAMETERS FOR THE SOFT HAPTIC DEVICE MODEL

Symbol	Description
P	Input air pressure
L_o	Initial actuator length
L_s	Initial actuator stretch length
ΔL	Lateral displacement of tactor head
H_{out}, W_{out}	Outer height and width of actuator
H_{in}, W_{in}	Inner height and width of actuator
A_o	Initial nominal cross sectional area
A	Nominal cross section area after deformation
λ	Stretch ratio
$F_{m,k}$	Material force generated by lateral actuator
$F_{p,k}$	Lateral actuator force generated by pressure
F_n	Normal indention force of tactor
$F_{s,k}$	Shear force of tactor
G	Young's modulus of the soft material
$(\,)_k$	k=l (left actuator), k=r (right actuator)

the product of input pressure and the cross sectional area of the inner cavity, which we assume remains constant.

The lateral actuators are pre-stretched, so they are under tension, as shown in Fig. 4(c). For modeling shear displacement, the initial stretched length of each side actuator is L_s. Since the actuator is made of incompressible soft material, the stretch ratio λ is

$$\lambda = L_s/L_o = A_o/A, \tag{2}$$

which is a ratio between the change in length and change in area.

When the silicone is stretched or compressed, material forces are generated, which force the tactor back towards the center. The material force F_m is

$$F_m = GA, \tag{3}$$

where G is the Young's modulus of the soft material used for the actuators.

While material forces push the tactor back towards the center, pressure forces move the tactor away from the center causing lateral displacements. The pressure force F_p is

$$F_p = P(H_{out}W_{out} - A), \tag{4}$$

and is a function of pressure and the nominal cross sectional area.

When the left actuator is pressurized, the tactor moves the distance ΔL to the right, as shown in Fig. 4(d). The total length of the tactor is fixed, so the length of the left actuator will be $L_s + \Delta L$ and the right actuator will be $L_s - \Delta L$. The force balance equation is thus

$$\begin{aligned} F_{s,l} &= F_{s,r} \\ F_{p,l} + F_{m,l} &= F_{m,r} \\ P(H_{out}W_{out} - A_l) + GA_l &= GA_r, \end{aligned} \tag{5}$$

which accounts for the pressurized actuator's pressure force and the material forces of both actuators. In this case, $A_l = AL_o/(L_s + \Delta L)$ is the cross sectional area of the left (pressurized) actuator and $A_r = AL_o/(L_s - \Delta L)$ is the cross sectional area of the right (unpressurized) actuator. Given a pressure input P, the displacement ΔL can be found from Eqn. 5.

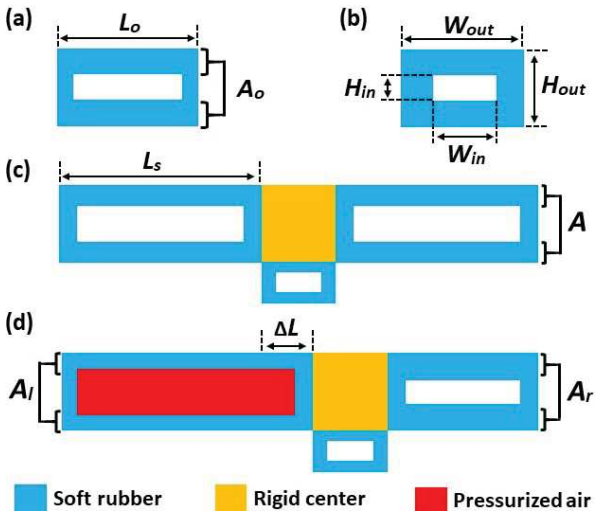

Fig. 4. The geometric parameters of the soft tactor model are shown for (a) a side-view of the lateral actuator without deformation, (b) a cross-sectional view of the lateral actuator without deformation, (c) the tactor at its pre-stretched state, and (d) the final tactor state with a pressurized left lateral actuator.

B. Model Validation

Table II shows the parameters obtained from the device used to test the accuracy of our model. According to the data sheet, the Young's modulus of Ecoflex 00-30 is 0.125 MPa. However, tensile testing using a dog bone sample shows that the function between the stretch ratio and the material stress is extremely nonlinear and yields a much smaller Young's Modulus around our initial stretch ratio of 2 [17]. Therefore, 0.075 MPa was used as the Young's Modulus for the model because it provided the best approximation for the stretch ratio of 1.5 to 3 that was used in the device. To measure the forces created by the haptic device, a 6-axis force/torque sensor (ATI, Nano 17) was placed beneath the the soft tactor head when when the device was actuated. This allowed the tactor head to slide on the sensor for force measurements.

Figure 5 compares the modeled normal force (Eqn. 1) to the measured normal force as the normal actuator is pressurized ($n = 4$). The standard deviation was within 1% of the mean, thus the forces are highly repeatable. From 0 to 3.5 psi, the model and experimental results match very closely. However, as the pressure in the normal actuator increases beyond 3.5 psi, the experimental results diverge from the model. Because the tactor is constrained between the force sensor and the guide rail, the soft material of the normal actuator expands, causing an increase in cross sectional area and thus, normal force given that the pressure is constant and

TABLE II

MEASURED VALUES USED FOR THE SOFT HAPTIC DEVICE MODEL

Symbol	Value	Unit
L_o	12.20	mm
H_{out}	7.70	mm
W_{out}	12.20	mm
H_{in}	6.10	mm
W_{in}	3.84	mm
L_s	22.60	mm
G	0.075	MPa

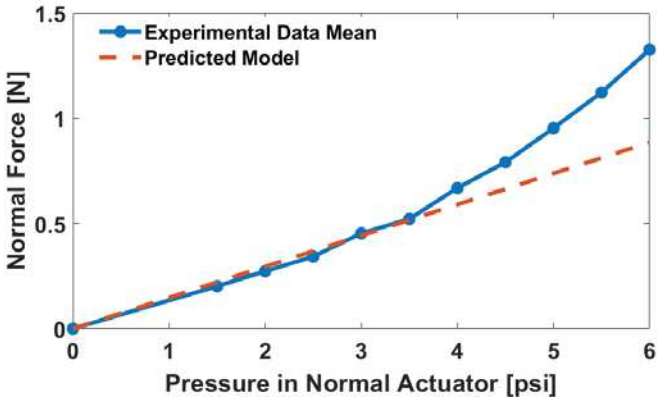

Fig. 5. The normal force generated by the tactor increases with the normal actuator pressure. The blue solid line is the experimental result and the red dashed line is the model output. The standard deviation (not shown) was within 1% of the mean ($n = 4$ for all measured pressures).

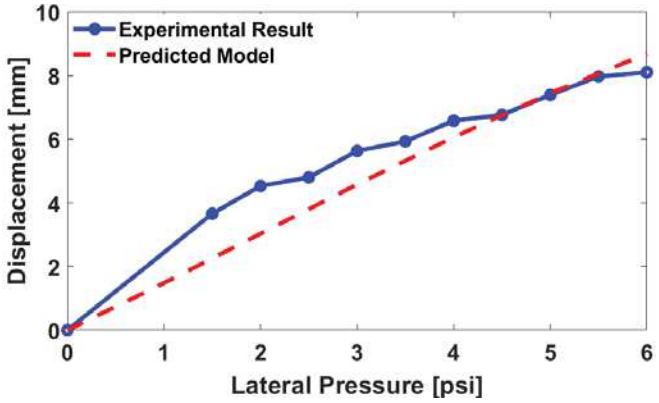

Fig. 6. Lateral actuator displacement increases with pressure. The blue solid line is the experimental result and the red dashed line is the predicted model. The displacement lengths were measured using calipers (error of +/- 0.03 mm).

$P = F/A$. At these high pressures, it is increasingly difficult to model forces by using this analytical solution.

Figure 6 shows the analytical and experimental values for tactor shear displacement. Calipers were used to measure the displacement of the tactor center when one lateral actuator is pressurized. The model predicted that the pressure of the lateral actuator directly relates to displacement, which is confirmed in the experimental result. However, the linear analytical model diverges from the experimental output due to the non-linearities in the soft actuator material properties.

Shear force data (Fig. 7) was collected by measuring peak lateral forces after pressurizing one lateral soft actuator, while the normal actuator pressure was 2, 4, or 6 psi. Because the coefficient of friction is constant, an increase in normal pressure would induce an increase in friction, and thus shear force, which is shown in the data. Additionally, When conducting experiments, the tactor tilted on the force sensor surface due to the moment created by the lateral actuator, rather than sliding on the sensor surface, explaining why the shear forces decrease with a smaller lateral pressure input. Due to the friction generated, at high lateral actuator pressures and low normal actuator pressures, the tactor produces a skin slip rather than a skin stretch. Because of this characteristic, in the future the device could implement cues via skin stretch or skin slip. These conditions are also highly repeatable, given that the standard deviation of the shear force was within 1% of the mean ($n = 4$).

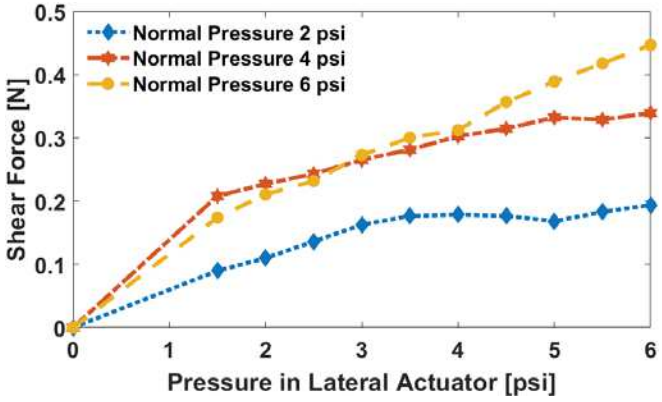

Fig. 7. The shear force generated by the tactor head can be as high as 0.47 N. The dashed lines indicate the shear forces from the experimental results using normal pressures of 2, 4, and 6 psi. The standard deviation (not shown) was within 1% of the mean ($n = 4$ for all measured pressures).

V. Haptic Modes

The device has multiple haptic modes in which it can provide feedback by using both its soft and rigid components. The combination of patterns through rotation and actuation in a 3-DoF device allows the tactor to move to multiple locations and orientations for stimulation while also avoiding unnecessary skin contact.

For example, the soft actuators can be pressurized and depressurized in sequence to create a stroking motion as shown in Fig. 8. First, the right side is pressurized to move the tactor head left. Second, the center actuator is pressurized to create contact with the surface. Third, a sweeping action creates a shear force as the left actuator pressurizes and the right actuator depressurizes. Last, the normal actuator is depressurized, allowing for skin contact to cease so that the actuator can return to its neutral position as shown in Fig. 3. This is an improvement over the previous device [3] which remained in contact with the skin, causing users to perceive additional cues when the tactor returned to its center position. The lateral motion created in the first step before creating contact with the skin also allows the device to increase the path of stimulation on the skin by a factor of two to 16 mm compared to just 8 mm. Additionally, the pressure of the normal actuator can be increased to provide skin stretch cues instead of skin slip cues by increasing normal pressure, and thus frictional forces affecting tactor end effector displacement.

Figure 9 shows the rotation of the inner rotational housing used to orient the shear movement of the soft tactor towards a particular angle. The order in which actuators are pressurized can be manipulated to create two different stroke angles at a single angular position of the device to simplify movements. For example, a shear force at 0° and 360° could have the same device angle, but an opposite stroking motion sequence by reversing the order of pressurization and depressurization of the actuators.

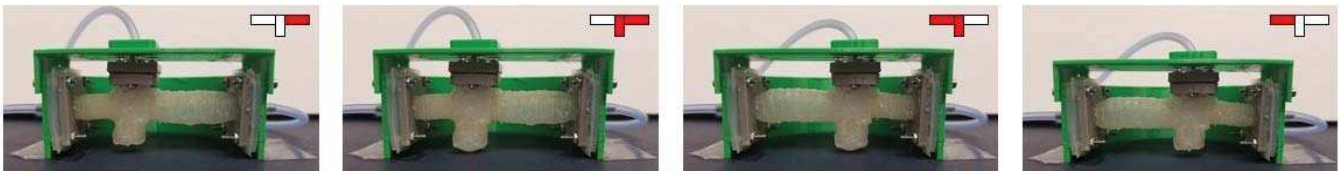

Fig. 8. The sequence for shear displacement is achieved by pressurizing and depressurizing various combinations of soft actuators. When performed in this pattern, they create a stroking cue on the forearm that can create skin stretch or slip. In the top right hand corner of each image, the pressurized actuators are shown in red, and the depressurized actuators are shown in white. The input pressure in these examples were 5 psi.

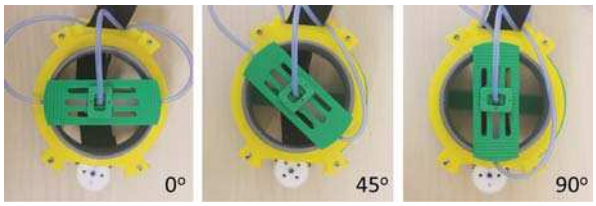

Fig. 9. The inner rotational housing of the haptic device, powered by a DC motor, can orient the tactor to a specific angle.

In summary, the device can provide:

- *Shear Cues* - Pressurizing the linear and normal actuators to create a sweeping motion.
- *Normal Cues* - Pressurizing the normal actuator to indent the skin.
- *Torsion Cues* - Pressurizing or depressurizing the normal actuator, then spinning the rotational housing.
- *Vibration Cues* - Generating oscillatory motor patterns.

In the future, these device modes can be combined to generate other stimulation patterns on the skin, such as creating circular shear on the skin by spinning the motor and pressurizing the normal and lateral actuator.

VI. Conclusion and Future Work

This work introduces a new wearable haptic device capable of providing normal, shear, vibration, and torsion cues. Compared to previous soft haptic devices, multiple modes of stimulation are created by using a pneumatic and electrical DC motor-driven system. This work also introduces a static displacement and force model for the tactor. The accuracy of this model was verified through experiments and allows design optimization for haptic requirements.

In the future, experiments to quantify the range of vibration and torque cues produced by the device will be examined. A user study will also be conducted to characterize users' ability to identify cues from the device. The limits of what cues and patterns generated from the device can be perceived will be evaluated to determine how the device can be used for guidance or communication. By understanding the cues users can detect , we can optimize model parameters to display a desired force or displacement and improve future devices.

To better control the actuators, sensors can also be integrated into the tactor head to enable closed-loop feedback control, allowing motions and forces to be controlled for haptic cues. The ability to both model and control soft actuators would prove useful towards the improvement of soft haptic and robotic devices.

References

[1] E. Y. Wong, A. Israr, and M. K. O'Malley, "Discrimination of consonant articulation location by tactile stimulation of the forearm," in *IEEE Haptics Symposium*, 2010, pp. 47–54.

[2] A. A. Stanley and K. J. Kuchenbecker, "Evaluation of tactile feedback methods for wrist rotation guidance," *IEEE Transactions on Haptics*, vol. 5, no. 3, pp. 240–251, 2012.

[3] S. Kanjanapas, C. M. Nunez, S. R. Williams, A. M. Okamura, and M. Luo, "Design and analysis of pneumatic 2-dof soft haptic devices for shear display," *IEEE Robotics and Automation Letters*, vol. 4, no. 2, pp. 1365–1371, 2019.

[4] M. Karam, F. A. Russo, and D. I. Fels, "Designing the model human cochlea: An ambient crossmodal audio-tactile display," *IEEE Transactions on Haptics*, vol. 2, no. 3, pp. 160–169, 2009.

[5] M. Kim, S. Lee, and S. Choi, "Saliency-driven real-time video-to-tactile translation," *IEEE Transactions on Haptics*, vol. 7, no. 3, pp. 394–404, 2014.

[6] H. Culbertson, C. M. Nunez, A. Israr, F. Lau, F. Abnousi, and A. M. Okamura, "A Social Haptic Device to Create Continuous Lateral Motion Using Sequential Normal Indentation," in *IEEE Haptics Symposium*, 2018, pp. 32–39.

[7] K. O. Johnson, "The roles and functions of cutaneous mechanoreceptors," *Current Opinion in Neurobiology*, vol. 11, no. 4, pp. 455–461, 2001.

[8] F. McGlone, J. Wessberg, and H. Olausson, "Discriminative and affective touch: Sensing and feeling," *Neuron*, vol. 82, no. 4, pp. 737–755, 2014.

[9] N. Dunkelberger, J. Bradley, J. L. Sullivan, A. Israr, F. Lau, K. Klumb, F. Abnousi, and M. K. O'Malley, "Improving Perception Accuracy with Multi-sensory Haptic Cue Delivery BT - Haptics: Science, Technology, and Applications," in *EuroHaptics*, 2018, pp. 289–301.

[10] M. Raitor, J. M. Walker, A. M. Okamura, and H. Culbertson, "WRAP: Wearable, Restricted-Aperture Pneumatics for Haptic Guidance," in *IEEE International Conference on Robotics and Automation*, 2017, pp. 427–432.

[11] N. Agharese, T. Cloyd, L. H. Blumenschein, M. Raitor, E. W. Hawkes, H. Culbertson, and A. M. Okamura, "HapWRAP: Soft Growing Wearable Haptic Device," in *IEEE International Conference on Robotics and Automation*, 2018, pp. 1–5.

[12] H. A. Sonar and J. Paik, "Soft pneumatic actuator skin with piezoelectric sensors for vibrotactile feedback," *Frontiers in Robotics and AI*, vol. 2, p. 38, 2016.

[13] M. Paré, H. Carnahan, and A. M. Smith, "Magnitude Estimation of Tangential Force Applied to the Fingerpad," *Experimental Brain Research*, vol. 142, no. 3, pp. 342–348, 2002.

[14] E. Treadway, B. Gillespie, D. Bolger, A. Blank, M. O'Malley, and A. Davis, "The role of auxiliary and referred haptic feedback in myoelectric control," in *IEEE World Haptics Conference*, 2015, pp. 13–18.

[15] E. Battaglia, J. P. Clark, M. Bianchi, M. G. Catalano, A. Bicchi, and M. K. O'Malley, "The Rice Haptic Rocker: Skin stretch haptic feedback with the Pisa/IIT SoftHand," in *IEEE World Haptics Conference*, 2017, pp. 7–12.

[16] E. H. Skorina, M. Luo, W. Y. Oo, W. Tao, F. Chen, S. Youssefian, N. Rahbar, and C. D. Onal, "Reverse pneumatic artificial muscles (rPAMs): Modeling, integration, and control," *PloS One*, vol. 13, no. 10, p. e0204637, 2018.

[17] Y. Elsayed, A. Vincensi, C. Lekakou, T. Geng, C. Saaj, T. Ranzani, M. Cianchetti, and A. Menciassi, "Finite element analysis and design optimization of a pneumatically actuating silicone module for robotic surgery applications," *Soft Robotics*, vol. 1, no. 4, pp. 255–262, 2014.